waste

MDPI

Article

Efficient Al Recovery from Aluminum Dross with Simultaneous AlN Separation by a Mechanical Method

Yujie Xue [1], Mingqi Zhang [2], Jizhi Zhou [1,*] and Yufeng Zhang [1,*]

[1] School of Environmental Science and Technology, Nanjing Tech University, No. 30 Puzhunan Road, Nanjing 211816, China
[2] School of Environmental and Chemical Engineering, Shanghai University, No. 99 Shangda Road, Baoshan District, Shanghai 200444, China
* Correspondence: jizhi.zhou@njtech.edu.cn (J.Z.); zhangyuf99@126.com (Y.Z.); Tel.: +86-025-58139652 (J.Z. & Y.Z.)

Highlights:

What are the main findings?

- Metallic Al in aluminum dross was separated by a milling method via size control.
- Ball medias decreased the fraction of large particles. Metallic Al particle with a size of 0.15–2 mm were targeted, which improved Al recovery to 65%. Most AlN was collected simultaneously in particles with size < 0.425 mm.

What are the implications of the main finding?

- Size control of aluminum dross was achieved by ball milling.

Abstract: Aluminum dross (AD) is a hazardous waste that contains valuable metallic Al and reactive aluminum nitride (AlN). The intergrowth of Al and AlN presents a challenge to Al recovery and AlN removal. In the current work, a mechanical milling method was developed to separate Al and AlN. Steel bars and balls were used as grinding media. The AD particle size decreased after milling and was distributed in the ranges 0.425–2 mm, 0.15–0.425 mm, 0.08–0.15 mm, and <0.08 mm. The particle size distribution was affected by the ball milling media and grinding time. Steel ball media had a better grinding effect on particles > 2 mm. After ball milling, the Dp0.08–2 mm size fraction accounted for approximately 90%. With changes in particle size, the element content of AD varied: the fraction of metallic Al decreased, while the fraction of Si increased. Metallic Al mainly existed in particles with size > 0.425 mm, accounting for 48.5%. AlN mainly existed in Dp0.15–0.425 mm, accounting for 64.9%. The optimal milling conditions achieved a 65% Al recovery rate and a 90% AlN separation efficiency. This work provides a promising approach for highly efficient pretreatment for AD recovery and AlN elimination in industrial applications.

Keywords: Al recovery; AlN seperation; ball milling

Citation: Xue, Y.; Zhang, M.; Zhou, J.; Zhang, Y. Efficient Al Recovery from Aluminum Dross with Simultaneous AlN Separation by a Mechanical Method. *Waste* **2023**, *1*, 40–51. https://doi.org/10.3390/waste1010004

Academic Editor: Carlito Tabelin

Received: 2 August 2022
Revised: 9 September 2022
Accepted: 22 September 2022
Published: 26 September 2022

1. Introduction

Aluminum dross (AD) is the main byproduct of the aluminum waste recovery industry, i.e., the process of remelting primary AD waste for aluminum recovery and regeneration and aluminum alloy production [1]. AD is a hazardous waste with an Al content of 30–50%. The composition of AD mainly includes Al, AlN, Si, SiO_2, $MgAlO_4$ and other salts. Aluminum is the most abundant metallic element in the Earth's crust and has an excellent combination of chemical, mechanical and physical properties, which makes it suitable for many applications, such as cement, refractory matter, polyaluminum chloride (PAC), ceramics, concrete, geomaterial and alloys [2–4]. AD is mainly disposed of by landfill, and AlN reacts with H_2O to generate NH_3, which may be harmful to the environment [5,6].

Consequently, it is essential to remove AlN before landfill disposal. Developing a method for metallic Al recovery and AlN separation is a current research hotspot.

Two methods of AD treatment are used: (1) the pyrometallurgical method, which is the conventional method of treating AD to liberate metallic aluminum in the liquid state, and (2) the hydrometallurgical method, which involves the extraction of metallic aluminum from AD by converting it into aluminum salts and compounds. Metal extraction using the pyrometallurgical process gives a good metal recovery rate. In the case of a lower metallic content in the dross, the hydrometallurgical process is preferred [7]. Many studies have been performed on the utilization of AD, and some such studies were based on acid leaching and alkaline leaching [8–15] P. E. Tsakiridis et al. observed aluminum recovery during black dross hydrothermal treatment [2]. The leaching efficiency of aluminum reached 57.5% with strong NaOH solution (260 g/L) at 240 °C. Artur Kudyba et al. studied Al recovery from AD by a high-temperature melting process, and the metallic Al recovery efficiency reached 52% for Dp > 2 [16]. M. Türk et al. studied Al recovery by the NaOH leaching method [17]. The Al extraction rate ranged from 78.64% to 93.11% and from 78.35% to 91.99% for ground dross and as-received dross, respectively. Haigang Feng studied the leaching rate of aluminum in secondary AD (SAD) and optimized the pretreatment process by adding grinding and water leaching steps; the SAD total aluminum leaching efficiency reached approximately 28.70% [18]. This increase in efficiency is markedly higher than the loss of AlN because the Al in AlN only accounts for 19.35% of the total Al content in AD.

AlN removal is achieved by calcination or hydrotreatment. AlN can be transformed into Al_2O_3 and N_2 at temperatures over 1000 °C in air [19]. Bajare et al. applied calcination to remove AlN; the AlN content was lower than the minimum value for X-ray diffraction (XRD) analysis after calcining at 1100 °C, which meant that most of the AlN was removed [20]. Alternatively, Fengqin Liu et al. researched nitrogen removal methods, where an optimal alkali-catalyzed denitrification hydrotreatment of AD at 90 °C with a reaction time of 300 min, a 6:1 liquid–solid ratio (mL:g), a stirring speed of 300 r/min, and a particle size smaller than 150 mesh [21]. Under optimal leaching conditions, the nitrogen removal rate was 93.48%. It is noted that the removal efficiency of AlN is relative to the size of AD [22–27] Zhengping Zuo et al. studied the Al recovery rate and AlN removal rate for particle size ranges of 150–250 μm, 74–150 μm and <74 μm. The rate of Al recovery increased with decreasing particle size, the maximum recovery rate was 97%, and the AlN removal rate reached 90.25% for Dp74–150 μm [28]. Since both the recovery of Al in AD and removal of AlN depend on the size of AD particle, an approach to the simultaneous separation of Al and AlN is paid much attention, depending on the effect of particle size on the element distribution.

In this paper, a new method is proposed for metallic Al recovery and AlN separation. The method is ball milling. Metallic Al is ductile, and due to its abrasiveness, the surface of metallic Al can be crushed and recovered after ball milling. Metallic Al mainly exists in larger AD particles, which significantly improves the metallic Al recovery efficiency. Moreover, AlN mainly exists in finer AD particles after ball milling. Sorting AD particles by size will not only solve remediation problems but also improve the resource utilization efficiency of AD. Different grinding media have different types of contact with AD, which causes different results. In this study, the recoverable Al fraction of coarse AD particles and the AlN fraction of fine AD particles were improved by controlling the grinding media and grinding time.

2. Materials and Methods

2.1. Materials

The AD sample was directly collected from an Al-Si alloy refining process (a company in Zhejiang, China). The crystal phase of AD was determined by solid XRD and is shown in Figure 1; the predominant XRD patterns corresponded to Al-Si alloy, AlN, Silicon (Si), SiO_2, and $MgAlO_4$. This result suggests that Al was present in the form of alloy, Al oxide and AlN. The element contents of AD (inset table) included 41.6% Al, 3.92% N and 2.61%

Si. This result suggests an AlN content of approximately 11.5%, as N was predominant in the form of AlN. Given the O content of 35%, oxides in AD are assumed to be in the form of Al oxides such as $MgAlO_4$ and amorphous Al_2O_3. This is consistent with the results in other studies [27]. Correspondingly, the Al content in the oxide was no more than 15%, which suggested that the metallic Al content was near 20%. This assumption is in good agreement with the metallic Si/Al ratio in AD at approximately 0.13% [21].

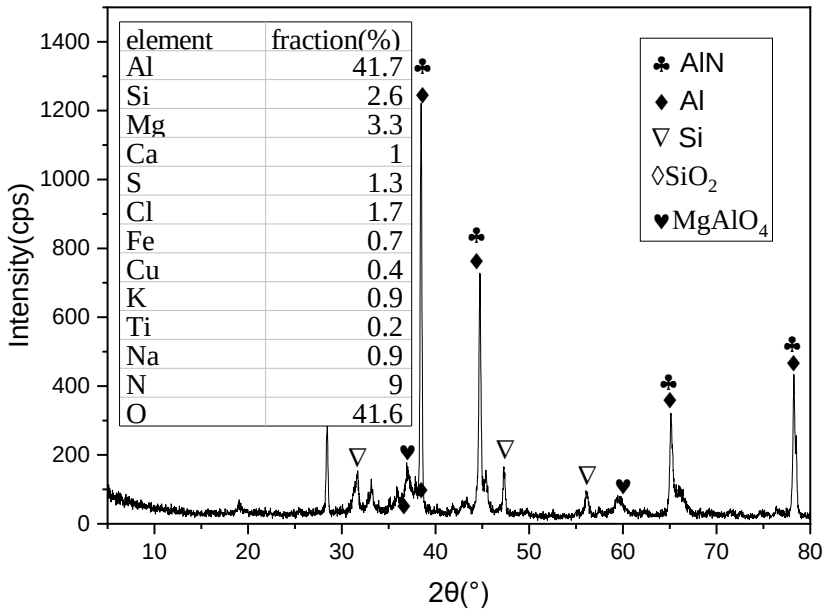

Figure 1. XRD pattern of AD with the element content (inner table).

2.2. Size Distribution

A 5.0 kg sample of AD was ground by a cement test mill with a steel ball (40 kg) or a steel bar (40 kg). After milling, the sample was screened via a series of sieves with sizes of 2 mm, 0.425 mm, 0.15 mm and 0.08 mm. The corresponding screened samples were collected for further characterization. Milling was conducted for 3, 5, or 10 min.

2.3. Composition Estimation

The changes in the amounts of Al and N in the solid sample were estimated by the following equations:

$$\mathrm{AlN}(\%) = \mathrm{W}_N/14 \times \mathrm{m}_{\mathrm{AlN}} \quad (1)$$

$$\mathrm{MetallicAl}(\%) = \gamma \mathrm{W}_{\mathrm{Si}} \quad (2)$$

where W_N is the percentage of N in the sample; m_{AlN} is the molecular weight of AlN; W_{Si} is the percentage of Si; and γ is an estimated weight coefficient of Al/Si for AD, which is suggested to be 7.5 (see details in the Supplemental Information).

2.4. Characterization Method

Element analysis of AD was performed by X-ray fluorescence spectroscopy (XRF-1800, Japan SHIMADZU LIMITED). The composition of solid samples was analyzed with an X-ray diffractometer (D/MAX2200 V PC, Neologi Electric Co., Ltd., Shanghai, China) with a scanning range of 5°–80° and a scanning speed of 8°/min. XRD analysis software MDI Jade 6.5 was used to index the diffraction peaks of the spectra and determine the composition.

The recoverable aluminum was determined by the furnace recovery method. AD was placed in a crucible and heated by high-frequency electric currents in an electromagnetic field to 700 °C. At high temperature, the aluminum metal in the dross melted and separated from other materials. After the melted portion was poured out, the aluminum liquid was

collected and cooled to obtain solid aluminum metal. The mass of the aluminum metal reflected the metal Al content in AD.

Nitrogen is mainly in the form of AlN in SAD. The content of AlN was obtained by measuring the concentration of nitrogen by Kjeldahl distillation. The ammonia produced in the conical flask was condensed by the reaction of alkali solution and AD, absorbed by boric acid solution and titrated with a standard solution of aminosulfonic acid. The mass fraction of nitrogen was calculated according to the consumption of aminosulfonic acid, and then the content of aluminum nitrite was calculated. The content of AlN was calculated by the following equation:

$$\mathrm{AlN}(\%) = 100 \times \mathrm{C} \times (\mathrm{V} - \mathrm{V}_0) \times 41/\mathrm{M} \quad (3)$$

where C represents the concentration of HCl, V represents the volume of consumed HCl, V_0 represents the volume of HCl in the blank experiment, and M represents the mass of AD.

3. Results and Discussion

3.1. Size Distribution

After sieving, the particle size distribution of raw AD followed the order > 2 mm, 0.425–2 mm, 0.15–0.425 mm, 0.08–0.15 mm, and <0.08 mm, whose morphology is shown in Figure S1. The corresponding percentages of these particle sizes were 22.3%, 30.8%, 23.7%, 21.1%, and 2.1%, respectively, as shown in Figure 2. Accordingly, the fractions with various particle sizes were defined as Dp > 2 mm, Dp 0.425–2 mm, Dp 0.15–0.425 mm, Dp 0.08–0.15 mm, and Dp < 0.08 mm, respectively.

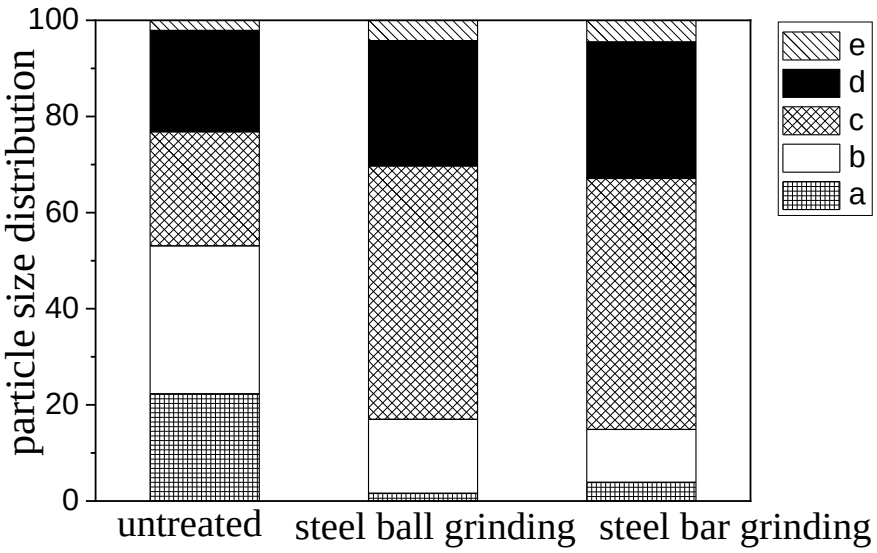

Figure 2. Particle size distribution of AD after milling with different grinding media (a: >2 mm, b: 0.425–2 mm, c: 0.15–0.425 mm, d: 0.08–0.15 mm, e: <0.08 mm).

Figure 2 illustrates the size distribution of AD particles after milling with different grinding media. After bar milling, the fraction of larger particles decreased, e.g., Dp > 2 mm declined to 1.6%, and Dp 0.425–2 mm decreased to 15.4%. In contrast, the fraction of Dp 0.15–0.425 mm increased to 52.7%. The fractions of Dp 0.08–0.15 mm and Dp < 0.08 mm slightly increased to 26.1% and 4.3%, respectively. A similar change in fractions for different particle size ranges was observed in the case of bar milling, which caused a dramatic increase in Dp 0.15–0.425 mm from 23.7% to 52.7% and a decrease in the fractions of Dp > 2 mm and Dp 0.425–2 mm. This result suggests that large particles of AD can be broken into smaller particles by grinding. It is proposed that metallic Al is probably separated from AlN, as metallic Al is more malleable than AlN. However, the size of some metallic Al may be decreased under mill treatment, which would lead to the combustion of

fine Al powder in thermal Al recovery. Kudyba et al. reported that a high recovery rate of Al was obtained when the size of Al was larger than 2 mm [16]. Therefore, the size of metallic Al should be controlled in mill processing.

In mill treatment, the grinding time plays an important role in the size of the product. Figure 3 shows the effect of grinding time on the AD particle size distribution. With increased steel bar milling time (Figure 3a), the fraction of larger particles decreased, e.g., Dp > 2 mm declined to 4.1%, and Dp 2–0.425 mm decreased to 31.5%. In contrast, the fraction of Dp0.425–0.15 mm increased to 35%, and that of Dp0.15–0.08 mm increased to 25.4%. The fraction of Dp < 0.08 mm slightly increased to 5.51% from 3 min grinding to 5 min grinding and then decreased to 4% with an increase in grinding time from 5 min to 10 min. This result suggests that the particle size of AD is mainly concentrated in the Dp2–0.15 mm range. Consequently, steel bar milling has the benefit of reducing the AD particle size. The particle size distribution changed steadily when the grinding time increased from 5 min to 10 min.

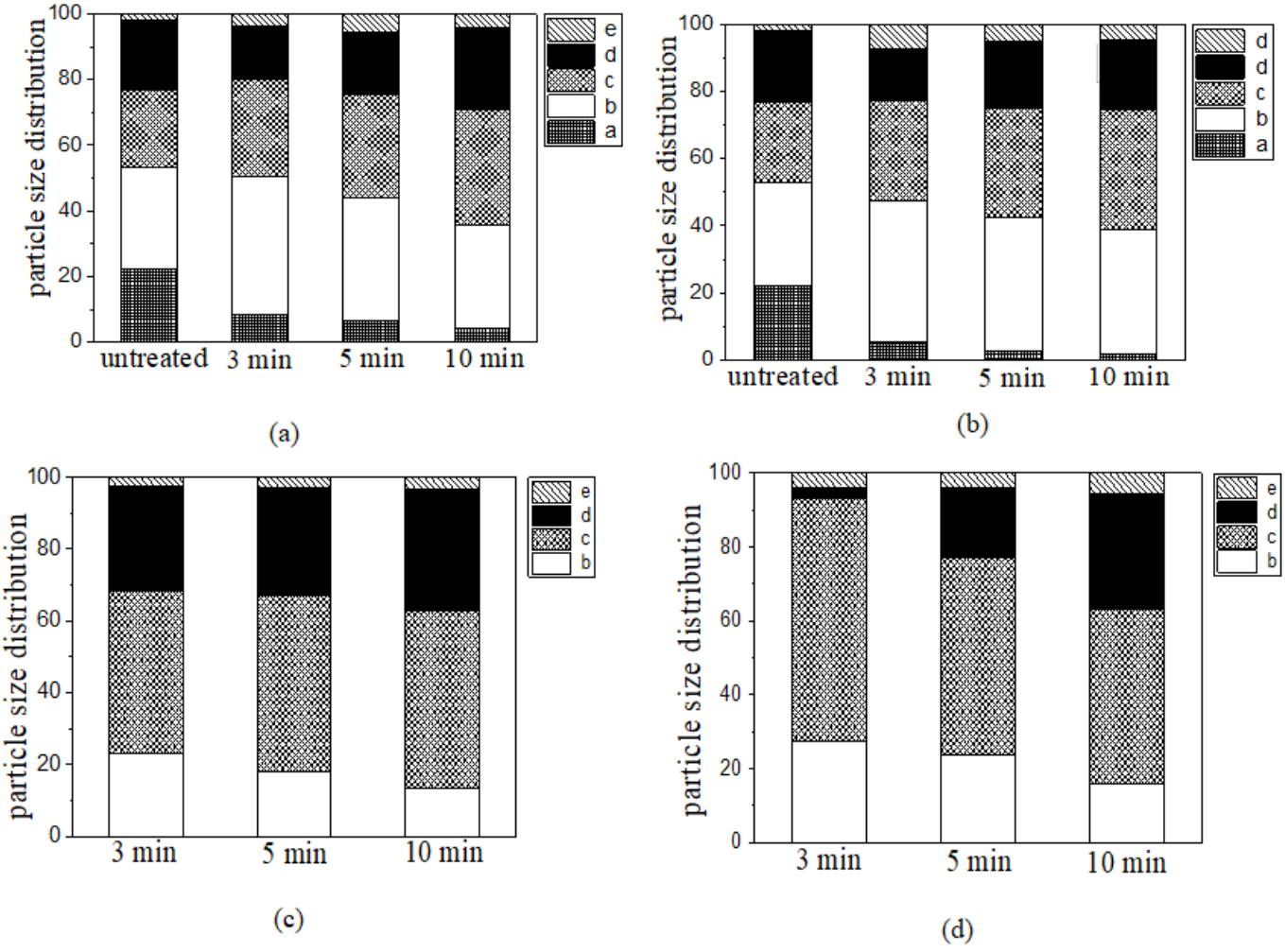

Figure 3. Particle size distributions obtained by (**a**) steel bar grinding and (**b**) steel ball grinding with (**c**,**d**) different times (a: >2 mm, b: 0.425–2 mm, c: 0.15–0.425 mm, d: 0.08–0.15 mm, e:<0.08 mm).

As shown in Figure 3b, the particle size distribution trend obtained by steel ball milling with different milling times exhibited a similar change in fractions to that obtained with bar milling. The fraction of larger particles decreased; e.g., the fraction of Dp > 2 mm decreased to 1.8%, and that of Dp2–0.425 mm decreased to 37%. In contrast, the fraction of Dp0.425–0.15 mm increased to 35.6%, and that of Dp0.15–0.08 mm increased to 20.9%. However, the fraction of Dp < 0.08 mm decreased to 4.7%. This result suggests that the

particle size of AD is mainly concentrated in the Dp2–0.15 mm range. The particle size distribution changed steadily when the grinding time increased from 5 min to 10 min, and the fraction of Dp > 2 mm was almost zero after 10 min of steel ball grinding. It can be concluded that the increase in ball milling time led to a decrease in the fraction of large AD particles (>2 mm). This result was in agreement with the result reported by S.S. Razavi-Tousi, where the particle size of AD was decreased to 44–74 μm with ball milling treatment. Consequently, ball milling has a greater benefit than bar milling with regard to reducing the size of large particles in AD.

To further investigate the effect of milling treatment on size distribution, a sample with a size < 2 mm was used in the milling process. The different particle size distributions of AD after different bar milling times are shown in Figure 4c. The particle size distribution was dominated by Dp0.425–0.15 mm after ball milling. As the bar milling time ranged from 3 min to 10 min, the fraction of larger particles decreased; e.g., the fraction of Dp2–0.425 mm AD decreased to 13.5%. In contrast, the fraction of Dp0.425–0.15 mm increased to 49.2%, and that of Dp0.15–0.08 mm increased to 33.8%. The fraction of Dp < 0.08 mm slightly increased to 3.5%. These results suggest that the particle size of AD is concentrated in the Dp0.425–0.15 mm range after steel bar grinding. With an increase in grinding time, the distribution of Dp < 0.425 mm did not significantly change, which indicates that steel bar grinding has little effect on Dp < 0.425 mm AD. Steel bar media is a reasonable option for grinding AD with coarse particle size.

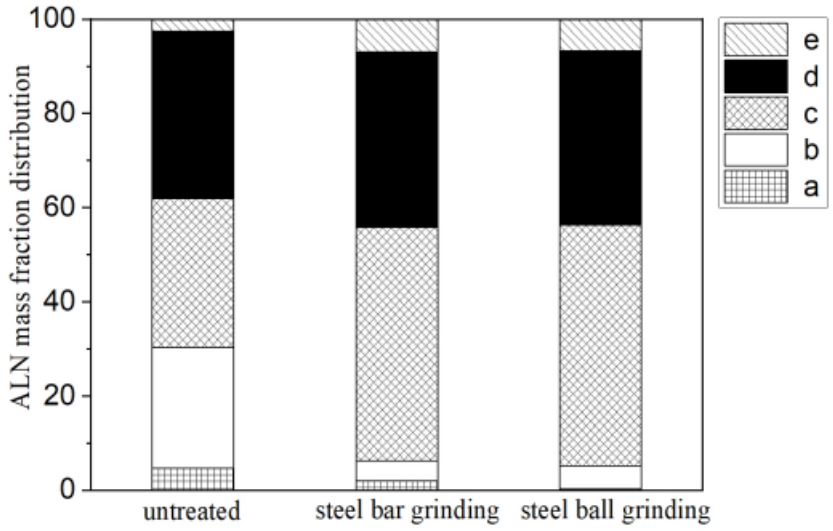

Figure 4. AlN mass fractions of different particle sizes of AD after ball milling or without treatment (a: >2 mm, b: 0.425–2 mm, c: 0.15–0.425 mm, d: 0.08–0.15 mm, e:<0.08 mm).

As shown in Figure 4d, the particle size was concentrated in the Dp0.425–0.15 mm range after steel ball milling. The fraction of larger particles decreased; e.g., the fraction of Dp2–0.425 mm decreased to 15.8%, and that of Dp0.425–0.15 mm decreased to 47.5%. In contrast, the fraction of Dp0.15–0.08 mm increased to 30.94%, and that of Dp < 0.08 mm increased to 5.79%. Compared to the case of bar milling, the higher amount of Dp < 0.08 mm and lower amounts of other size fractions suggest that steel ball media has a strong effect on the increase in fine particle size with increasing time. To increase Al recovery, it is important to keep the particle size at 0.15–2 mm. As a result, milling treatment should include a shorter time, and bar grinding media should be used. Therefore, 3 min was selected as the optimal grinding time.

3.2. Element Distribution

The element distribution of AD after different steel bar grinding times was analyzed. As shown in Table S1, the main elements in AD were Al and Si with steel bar grinding.

The Al fraction of Dp > 2 mm decreased to 29.8% and then increased to 36.9% with the increment of grinding time. In contrast, the Al fraction of Dp < 0.425 mm first increased, and then decreased. The Al fraction of Dp0.425–2 mm increased to 38.5% as the grinding time ranged from 3 min to 10 min. After steel bar grinding, Al fraction concentrated on Dp0.15–2 mm, indicating that Al of Dp > 2 mm had been ground into smaller particle sizes. The result suggests that the recoverable Al fraction increased after steel bar grinding compared with that of raw AD, indicating that steel bar grinding is a reasonable option for metallic Al recovery.

As shown in Table S2, the main elements of AD obtained by steel bar grinding were Al and Si. As the steel ball grinding time increased from 3 min to 10 min, the Al fraction of Dp > 2 mm decreased to 5.56%. In contrast, the Al fraction of Dp < 0.08 mm increased to 46.81%. The Al distribution concentrated on Dp0.15 = 2 mm. The Al fraction reached 55.67 at 5 min steel ball grinding. By comparison with the Al fraction data in Table S1, the Al fraction of Dp0.425–2 mm after steel ball grinding was higher than that with steel bar media, which indicates that steel ball media have a better metallic Al recovery efficiency.

The Si fraction of Dp > 2 mm increased to 13.5% as the steel bar grinding time increased from 3 min to 5 min. The Si fraction of Dp > 2 mm decreased to 10.2% as the steel bar grinding time ranged from 5 min to 10 min. The Si fraction of Dp2–0.425 mm decreased to 8.65% as the steel bar grinding time increased from 3 min to 5 min. The Si fraction of Dp2–0.425 mm slightly increased to 9.09% as the steel bar grinding time ranged from 5 min to 10 min. The Si fraction of Dp0.425–0.15 mm slightly increased to 8.56% as the steel bar grinding time ranged from 3 min to 10 min. The Si fraction of Dp0.15–0.08 mm decreased to 6.64% as the steel bar grinding time ranged from 3 min to 10 min. The Si fraction of Dp < 0.08 mm slightly decreased to 5.95% as the steel bar grinding time increased from 3 min to 5 min. The Si fraction of Dp < 0.08 mm slightly increased to 6.37% as the steel bar grinding time ranged from 5 min to 10 min. The Si distribution decreased with the decline of particle size, indicating that steel bar media has a worse grinding effect on monatomic silicon.

The Si fraction of different particle size has a similar change by steel ball grinding. However, the Si fraction increased with the decline of particle size, indicating that monatomic silicon had been ground into finer particle sizes by the steel ball media.

The mass fraction of elements with different steel bar grinding times is shown in Table 1. Compared with the contents of raw AD, the fraction of metallic Al decreased to 38.3% and that of Si increased to 8.2% after 10 min of steel bar grinding. The ball milling process causes the loss of the Al fraction. With decreasing particle size, the Al/Si ratio increased from 3.3 to 6.3 after 3 min steel bar grinding, from 2.2 to 6.6 after 5 min steel bar grinding, and from 3.6 to 6.1 after 10 min steel bar grinding. The change in Al/Si was not linear with increasing steel bar grinding time. The sum of the metallic Al fraction changed steadily after 5 min of steel bar grinding. Given the energy cost of milling, the optimal steel bar grinding time was 5 min for improving the metallic Al fraction.

Table 1. Mass fractions of elements obtained with steel bar grinding.

Time	Element	>2 mm	0.425–2 mm	0.15–0.425 mm	0.08–0.15 mm	<0.08 mm	Sum
3 min	Al (%)	2.9	15.0	11.2	6.4	1.4	36.9
	Si (%)	0.9	4.4	2.4	1.1	0.2	9.0
5 min	Al (%)	2.0	14.3	12.1	7.6	2.2	38.2
	Si (%)	0.9	3.2	2.5	1.3	0.3	8.3
10 min	Al (%)	1.5	12.1	13.2	10.0	1.6	38.3
	Si (%)	0.4	2.9	3.0	1.7	0.3	8.2

The mass fraction of elements with different steel ball grinding times is shown in Table 2. The mass fraction change of elements is similar to steel bar grinding. The Al/Si ratio decreased to 0.25 by 3 min steel ball grinding. In contrast, the Al/Si ratio increased to 1.55 after 5 min steel ball grinding and 2 after 10 min steel ball grinding. Consequently,

the ball milling method has a significant effect on the element distribution, making this approach a reasonable option for metallic Al recovery and impurity separation.

Table 2. Mass fractions of elements obtained with steel ball grinding.

Time	Element	>2 mm	0.425–2 mm	0.15–0.425 mm	0.08–0.15 mm	<0.08 mm	Sum
3 min	Al (%)	1.3	19.4	15.2	4.2	0.3	40.4
	Si (%)	0.3	3.2	1.8	1.9	1.2	8.4
5 min	Al (%)	0.4	22.1	10.6	5.3	1.7	40.1
	Si (%)	0.5	2.7	2.1	2.2	1.1	8.6
10 min	Al (%)	0.1	16.3	12.6	6.9	2.2	38.1
	Si (%)	0.1	2.8	3.1	1.9	1.1	9

Figure S2 shows the compositions of samples with various milling times as illustrated by the XRD patterns. When the steel bar grinding time was less than 5 min, Dp > 2 mm displayed the peak of SiO_2. In contrast, Dp < 2 mm presented the peaks of Al, AlN, Si, and $MgAlO_4$. The Al peak of Dp0.15–0.08 mm reached a maximum at a 3 min steel bar grinding time, while the Al peak of Dp0.425–0.15 mm reached a maximum at 5 min of steel bar grinding. On the basis of comparison with Figure 1, ball milling achieves the separation of Al from SiO_2 slag, which indicates that metallic Al contained in slag can be recovered by smelting. The peaks of Al, AlN, Si, and $MgAlO_4$ for the Dp < 2 mm fraction were similar to those corresponding to less than 5 min steel bar grinding, while the peak of Al_2O_3 of Dp > 2 mm was observed after 10 min steel bar grinding, which indicated that Al may react with oxygen to generate Al_2O_3. Considering the above result, the phases can be separated by grinding for a short time, and the size of AD and the metallic Al recovery efficiency decreased with increasing grinding time.

AlN exists in fine-particle size AD, indicating that ball milling can reduce the size of AlN. On the basis of comparison with Figure 1, metallic Al and AlN can be separated after ball milling, which indicates that ball milling promoted a difference in the distributions of metallic Al and AlN. Consequently, the ball milling method is a reasonable option for metallic Al recovery and AlN separation.

Figure S3 shows SEM-EDS of different particle size; two plots were chosen to distinguish AlN and metallic Al. As shown in Figure S3, Dp < 0.08 mm includes Al and N, indicating that AlN mainly exists in Dp < 0.08 mm. In the contrary case, where Dp > 0.08 mm, the AD only exists as element Al, indicating that metallic Al exists primarily here in large particle size. The Al fraction varies from different plots, larger particle size has higher Al fraction. The result is available for further experiments.

3.3. Aluminum Recovery (Recoverable Aluminum Metal)

The recovery quality of metallic Al was obtained from a high frequency furnace recovery method. The metallic Al fraction of different particle size ranges obtained with different steel ball grinding times is shown in Table 3. As the steel ball grinding time ranged from 3 min to 10 min, the metallic Al fraction of Dp > 2 mm decreased to 0.03%, that of Dp2–0.425 mm decreased to 14.47%, and that of Dp < 0.08 mm decreased to 0.24%. In contrast, the metallic Al fraction of Dp0.425–0.15 mm increased to 13.41%, and that of Dp0.15–0.08 mm increased to 4.62%. The metallic Al fraction of different particle size ranges obtained with different steel bar grinding times is illustrated in Table S3. In contrast to the results of steel ball grinding, the metallic Al fraction of Dp < 0.08 mm increased to 0.31% with increased grinding time. As the steel bar grinding time changed, the metallic Al fraction of Dp2–0.425 mm decreased to 10.50% and then increased to 12.87%. In contrast, the metallic Al fraction of Dp0.425–0.15 mm increased to 10.85% and then decreased to 10.57%. The metallic Al fraction of Dp > 2 mm decreased, indicating that metallic Al fraction of Dp > 2 mm was transformed into finer particle size. With the increment of grinding time, the metallic Al of Dp0.425–2 mm AD was transformed into a finer particle, which leads to the decline of metallic Al fraction.

Table 3. Metallic Al contents of different particle sizes of AD after various steel ball grinding times.

Grinding Time	>2 mm	0.425–2 mm	0.15–0.425 mm	0.08–0.15 mm	<0.08 mm	Sum
3 min (%)	0.30	19.91	9.96	2.61	0.59	33.37
5 min (%)	0.07	16.96	11.56	4.17	0.29	33.06
10 min (%)	0.03	14.47	13.41	4.62	0.24	32.77

The total metallic Al fraction did not significantly change after ball milling. Compared with the content of raw AD, the total metallic Al fraction after steel ball grinding decreased to 32.77%, and that after steel bar grinding decreased to 26.94%, indicating that some metallic Al was lost during the ball milling process. This result suggests that the metallic Al fraction is concentrated in the Dp2–0.15 mm range, which is available for metallic Al recovery. As a result, Dp2–0.15 mm was selected for the subsequent metallic Al recovery experiment.

The metallic Al recovery fraction of Dp2–0.15 mm obtained by steel ball grinding is illustrated in Table S4. With increased steel ball grinding time, the metallic Al fraction of Dp2–0.425 mm increased to 25.40%, and that of Dp0.425–0.15 mm increased to 7.99%. In contrast, the metallic Al fraction of Dp2–0.425 mm decreased to 17.7%, while that of Dp0.425–0.15 mm increased to 4.49%, as the steel bar grinding time ranged from 3 min to 10 min, as shown in Table S5. The metallic Al recovery rates obtained by steel ball grinding are shown in Table S6. The metallic Al recovery rate of Dp2–0.425 mm increased to 64.9% and that of Dp0.425–0.15 mm increased to 37.7% as the steel ball grinding time ranged from 3 min to 10 min. In contrast, the maximum metallic Al recovery rate of Dp2–0.425 mm was 56.9% at a 5 min steel bar grinding time, and the maximum metallic Al recovery of Dp0.425–0.15 mm was 14.9% at 10 min of steel bar grinding, as shown in Table S7. Considering the above results, steel ball media has a better metallic Al recovery rate than steel bar media. The optimal condition for metallic Al recovery was 10 min of steel ball grinding.

The treatment of AD by steel ball milling separated richer and larger metallic Al-containing particles from finer and richer nonmetallic particles. The metallic Al recovery rate reached approximately 65% with steel ball grinding. It is worth mentioning that using steel ball media is the cheapest industrial process in the mineral industry, and it does not require high capital expenses (CAPEX) or operational expenses (OPEX) compared to other mineral processing techniques. Hence, the application of this methodology is feasible, as it has been used for many years in different industries and does not require technology development or high expertise levels.

3.4. Simultaneous AlN Separation

AlN is the harmful component of AD, and AlN reacts with H_2O to generate NH_3, which causes air pollution. Ammonia is an alkaline substance, corrosive and irritating. Consequently, it is essential to separate AlN before comprehensive utilization of AD. Currently, AlN is removed by reaction with oxygen to generate NO and NO_2, which avoids NH_3 generation. In this paper, a new approach was adopted to separate AlN. The method separates AlN by ball milling, which leads to the aggregation of AlN in fine-particle size AD.

Figure 4 shows the AlN fraction of different particle sizes of AD with different grinding media. Compared with raw AD, the AlN fraction of Dp > 2 mm AD decreased to 2.0%, and that of Dp2–0.425 mm decreased to 4.3%. In contrast, with steel bar grinding, the AlN fraction of Dp0.425–0.15 mm AD increased to 49.5%, that of Dp0.15–0.08 mm increased to 37.2% and that of Dp < 0.08 mm AD increased to 7.0%. Similar changes in the AlN fractions of different particle sizes were observed after steel ball grinding. The AlN fraction of Dp > 2 mm AD decreased to 0.2%, and that of Dp2–0.425 mm AD to 5.0%. In contrast, after steel ball grinding, the AlN fraction of Dp0.425–0.15 mm AD increased to 51.0%, that of Dp0.15–0.08 mm AD increased to 37.0%, and that of Dp < 0.08 mm AD increased to 6.7%.

Considering the above results, larger AD particles were broken into smaller particles, which led to an increase in the AlN fraction of smaller particles after steel ball grinding. This result suggests that AlN can be separated from larger-particle size AD after steel ball grinding.

The AlN fractions of different particle sizes obtained by steel ball grinding are illustrated in Table 4. As the steel ball grinding time increased from 3 min to 10 min, the AlN fraction of Dp > 2 mm decreased to zero, that of Dp2–0.425 mm decreased to 1.84%, and that of Dp < 0.08 mm decreased to 0.32%. In contrast, the AlN fraction of Dp2–0.425 mm increased to 18.17%, and that of Dp0.15–0.08 mm increased to 7.73%. Similar changes were observed after steel bar grinding, as shown in Table S8. The AlN fraction of Dp > 2 mm decreased to 0.08%, and that of Dp2–0.425 mm decreased to 1.35%. In contrast, the AlN fraction of Dp0.425–0.15 mm increased to 17.33%, and that of Dp0.15–0.08 mm increased to 9.45%. The AlN fraction of Dp < 0.08 mm first increased to 0.38% and then decreased to 0.28% as the steel bar grinding time increased from 3 min to 10 min. The AlN remained concentrated on Dp0.08–0.425 mm. AlN exists on the surface of larger particle size, but appeared among finer particle sizes after milling treatment, which leads to the AlN increment of finer particle size.

Table 4. AlN fractions of different particle sizes obtained by steel ball grinding.

Grinding Time	>2 mm	0.425–2 mm	0.15–0.425 mm	0.08–0.15 mm	<0.08 mm	Sum
3 min (%)	0.01	2.11	15.26	5.66	0.49	23.53
5 min (%)	0.01	1.98	16.74	7.29	0.35	26.36
10 min (%)	0.00	1.84	18.17	7.73	0.32	28.06

Considering the above results, AlN is concentrated in Dp0.425–0.15 mm and Dp0.15–0.08 mm after steel ball grinding. This result suggests that metallic Al and AlN were separated after steel ball grinding.

4. Conclusions

Al recovery and AlN separation from AD were studied experimentally via ball milling. The following conclusions were drawn from this work:

(1) The fraction of Dp < 0.08 mm in untreated AD is lower, while the fraction of other particle sizes of AD is uniform. After ball milling, the particle size distribution is centered at Dp0.425–0.08 mm AD. Grinding with steel bar and steel ball media has obvious impacts on coarse AD particles. Steel ball grinding media have a better impact than steel ball media.
(2) After ball milling, the element fractions of different particle sizes of AD vary. Metallic Al is concentrated in the Dp2–0.425 mm fraction of AD, and AlN is concentrated in the Dp0.425–0.15 mm fraction of AD.
(3) The metallic Al recovery rate reached 65% after 10 min of steel ball grinding.
(4) The AlN mass fraction reached approximately 90% after 10 min of steel ball grinding.

Supplementary Materials: The following supporting information can be downloaded at: https://www.mdpi.com/article/10.3390/waste1010004/s1, Figure S1: Secondary aluminum dross sieving size range; Table S1: element distribution of different particle sizes aluminum dross after different steel bar grinding time; Table S2: element distribution of different particle sizes aluminum dross after different steel ball grinding time; Figure S2: Results of XRD analyses of different particle sizes of AD after steel bar grinding; Figure S3: SEM-EDS of different particle size; Table S3: Subentry metallic Al content of different particle sizes aluminum dross after steel bar grinding time; Table S4: recoverable metallic Al fraction by steel ball grinding; Table S5: recoverable metal Al fraction by steel bar grinding; Table S6: Al recovery rate of total Al by steel ball grinding; Table S7: Al recoverable rate of total Al by steel bar grinding; Table S8: AlN fraction of different particle size by steel bar grinding.

Author Contributions: Conceptualization, J.Z., Y.Z.; Methodology, J.Z., Y.Z.; Resources, J.Z.; Data Curation, J.Z.; Writing—Original Draft, Y.X.; Visualization, Y.X.; Investigation, M.Z. All authors have read and agreed to the published version of the manuscript.

Funding: This research received no external funding.

Institutional Review Board Statement: Not applicable.

Informed Consent Statement: Not applicable.

Data Availability Statement: Not applicable.

Conflicts of Interest: The authors declare no conflict of interest.

References

1. Mahinroosta, M.; Allahverdi, A. A promising green process for synthesis of high purity activated-alumina nanopowder from secondary aluminum dross. *J. Clean. Prod.* **2018**, *179*, 93–102. [CrossRef]
2. Tsakiridis, P.E. Aluminium salt slag characterization and utilization—A review. *J. Hazard. Mater.* **2012**, *217–218*, 1–10. [CrossRef] [PubMed]
3. Elseknidy, M.; Salmiaton, A.; Shafizah, I.N.; Saad, A. A Study on Mechanical Properties of Concrete Incorporating Aluminum Dross, Fly Ash, and Quarry Dust. *Sustainability* **2020**, *12*, 9230. [CrossRef]
4. Lin, Y.; Maghool, F.; Arulrajah, A.; Horpibulsuk, S. Engineering Characteristics and Environmental Risks of Utilizing Recycled Aluminum Salt Slag and Recycled Concrete as a Sustainable Geomaterial. *Sustainability* **2021**, *13*, 10633. [CrossRef]
5. Hong, J.-P.; Wang, J.; Chen, H.-Y.; Sun, B.-D.; Li, J.-J.; Chen, C. Process of aluminum dross recycling and life cycle assessment for Al-Si alloys and brown fused alumina. *Trans. Nonferrous Met. Soc. China* **2010**, *20*, 2155–2161. [CrossRef]
6. Shen, H.; Forssberg, E. An overview of recovery of metals from slags. *Waste Manag.* **2003**, *23*, 933–949. [CrossRef]
7. Meshram, A.; Singh, K.K. Recovery of valuable products from hazardous aluminum dross: A review. *Resour. Conserv. Recycl.* **2018**, *130*, 95–108. [CrossRef]
8. Li, A.; Zhang, H.; Yang, H. Evaluation of aluminum dross as raw material for high-alumina refractory. *Ceram. Int.* **2014**, *40*, 12585–12590. [CrossRef]
9. Li, J.; Wang, J.; Chen, H.; Sun, B. Microstructure observation of β-sialon-15R ceramics synthesized from aluminum dross. *Ceram. Int.* **2012**, *38*, 3075–3080. [CrossRef]
10. Mahinroosta, M.; Allahverdi, A. Hazardous aluminum dross characterization and recycling strategies: A critical review. *J. Environ. Manag.* **2018**, *223*, 452–468. [CrossRef]
11. Xiao, Y.; Reuter, M.; Boin, U. Aluminium recycling and environmental issues of salt slag treatment. *J. Environ. Sci. Health A Tox. Hazard. Subst. Environ. Eng.* **2005**, *40*, 1861–1875. [CrossRef] [PubMed]
12. Hiraki, T.; Miki, T.; Nakajima, K.; Matsubae, K.; Nakamura, S.; Nagasaka, T. Thermodynamic Analysis for the Refining Ability of Salt Flux for Aluminum Recycling. *Materials* **2014**, *7*, 5543–5553. [CrossRef] [PubMed]
13. Zhang, Y.; Guo, Z.; Han, Z.; Xiao, X. Effect of rare earth oxides doping on $MgAl_2O_4$ spinel obtained by sintering of secondary aluminium dross. *J. Alloys Compd.* **2018**, *735*, 2597–2603. [CrossRef]
14. Yoshimura, H.; Abreu, A.; Molisani, A.L.; de Camargo, A.C.; Portela, J.; Narita, N. Evaluation of aluminum dross waste as raw material for refractories. *Ceram. Int.* **2008**, *34*, 581–591. [CrossRef]
15. Roy, R.R.; Sahai, Y. Interfacial tension between aluminum alloy and molten salt flux. *Mater. Trans. JIM* **1997**, *38*, 546–552. [CrossRef]
16. Kudyba, A.; Akhtar, S.; Johansen, I.; Safarian, J. Aluminothermic Reduction of Manganese Oxide from Selected MnO-Containing Slags. *Materials* **2021**, *14*, 356. [CrossRef]
17. Türk, M.; Altıner, M.; Top, S.; Karaca, S.; Bouchekrit, C. Production of Alpha-Alumina from Black Aluminum Dross Using NaOH Leaching Followed by Calcination. *JOM* **2020**, *72*, 3358–3366. [CrossRef]
18. Feng, H.; Zhang, G.; Yang, Q.; Xun, L.; Zhen, S.; Liu, D. The Investigation of Optimizing Leaching Efficiency of Al in Secondary Aluminum Dross via Pretreatment Operations. *Processes* **2020**, *8*, 1269. [CrossRef]
19. Lin, C.-Y.; Lu, F.-H. Oxidation behavior of AlN films at high temperature under controlled atmosphere. *J. Eur. Ceram. Soc.* **2008**, *28*, 691–698. [CrossRef]
20. Bajare, D.; Korjakins, A.; Kazjonovs, J.; Rozenstrauha, I. Pore structure of lightweight clay aggregate incorporate with non-metallic products coming from aluminium scrap recycling industry. *J. Eur. Ceram. Soc.* **2012**, *32*, 141–148. [CrossRef]
21. Liu, F.; Zuo, Z.; Han, J.; Zhao, H.; Li, R. Removal Process and Kinetics of Nitrogen and Chlorine Removal from Black Aluminum Dross. *J. Sustain. Metall.* **2021**, *7*, 1805–1818. [CrossRef]
22. Gong, Y.; Sun, J.; Zhang, Y.; Zhang, Y.; Zhang, T.-A. Dependence on the distribution of valuable elements and chemical characterizations based on different particle sizes of high alumina fly ash. *Fuel* **2021**, *291*, 120225. [CrossRef]
23. Li, Y.; Qin, Z.; Li, C.; Qu, Y.; Wang, H.; Peng, L.; Wang, Y. Hazardous characteristics and transformation mechanism in hydrometallurgical disposing strategy of secondary aluminum dross. *J. Environ. Chem. Eng.* **2021**, *9*, 106470. [CrossRef]

24. Razavi-Tousi, S.S.; Szpunar, J.A. Mechanism of Corrosion of Activated Aluminum Particles by Hot Water. *Electrochim. Acta* **2014**, *127*, 95–105. [CrossRef]
25. Aziz, M.H.A.; Othman, M.H.D.; Hashim, N.A.; Rahman, M.A.; Jaafar, J.; Hubadillah, S.K.; Tai, Z.S. Pretreated aluminium dross waste as a source of inexpensive alumina-spinel composite ceramic hollow fibre membrane for pretreatment of oily saline produced water. *Ceram. Int.* **2019**, *45*, 2069–2078. [CrossRef]
26. Jiménez, A.; Misol, A.; Morato, Á.; Rives, V.; Vicente, M.A.; Gil, A. Synthesis of pollucite and analcime zeolites by recovering aluminum from a saline slag. *J. Clean. Prod.* **2021**, *297*, 126667. [CrossRef]
27. Ghorab, H.Y.; Rizk, M.; Matter, A.; Salama, A.A. Characterization and Recycling of Aluminum Slag. *Polym.-Plast. Technol. Eng.* **2004**, *43*, 1663–1673. [CrossRef]
28. Zuo, Z.; Lv, H.; Li, R.; Liu, F.; Zhao, H. A new approach to recover the valuable elements in black aluminum dross. *Resour. Conserv. Recycl.* **2021**, *174*, 105768. [CrossRef]